*Current Cancer Drug Targets*, 2022, *22*, 153-168

RESEARCH ARTICLE

# Promotion of Cervical Cancer Cell Proliferation by miR-130b Expression Level Changes and Inhibition of its Apoptosis by Targeting CDKN1A Gene

Yanli Wang[1,†], Lei Yang[2,†], Caihong Fan[3,†], Hong Mu[2,*], Munan Han[4], Tao Liu[5], Lili Xie[2] and Qiang Gao[2]

[1]*Department of Clinical Laboratory, Tianjin Hospital of ITCWM Nankai Hospital, Tianjin, China;* [2]*Department of Clinical Laboratory, Tianjin First Center Hospital, Tianjin, China;* [3]*The First Central Clinical College of Tianjin Medical University, Tianjin Medical University, Tianjin, China;* [4]*First Clinical Medical College, Nanjing Medical University, Nanjing, China;* [5]*Key Laboratory for Critical Care Medicine of the Ministry of Health, Tianjin, China*

**Abstract:** ***Background*:** Dysregulation of miR-130b expression is associated with the development of different cancers. However, the description of the biological roles of miR-130b in the growth and survival of cervical cancer cells is limited.

***Methods*:** The miR-130b levels in cervical cancer cells during different stages of growth were determined using reverse transcription-quantitative PCR. The methylation level of DNA sequences upstream of the miR-130b gene was measured using an SYBR Green-based quantitative methylation-specific PCR. Reverse transcription-quantitative PCR, Western blotting, and fluorescence report assays were used to identify the miR-130b-targeted gene. Cell counting kit-8 and comet assays were used to determine cell viability and DNA damage levels in cells, respectively. EdU Apoplo488 *in vitro* Flow Cytometry kit, propidium iodide staining, anti-γ-H2AX antibody staining, and Annexin-V apoptosis kit were subsequently used to determine DNA synthesis rates, cell cycle distribution, count of DNA double-strand breaks, and levels of apoptotic cells.

***Results*:** miR-130b levels increased at exponential phases of the growth of cervical cancer cells but reduced at stationary phases. The methylation of a prominent CpG island near the transcript start site suppressed the miR-130b gene expression. MiR-130b increased cell viability, promoted both DNA synthesis and G1 to S phase transition of the cells at exponential phases, but reduced cell viability accompanied by accumulations of DNA breaks and augmentations in apoptosis rates of the cells in stationary phases by targeting cyclin-dependent kinase inhibitor 1A mRNA.

***Conclusion*:** miR-130b promoted the growth of cervical cancer cells during the exponential phase, whereas it impaired the survival of cells during stationary phases.

ARTICLE HISTORY

Received: June 22, 2021
Revised: October 21, 2021
Accepted: November 12, 2021

*DOI:*
*10.2174/1568009622666220111090715*



**Keywords:** Dynamics, miR-130b, expression level changes, cervical cancer cell, growth, survival.

## 1. INTRODUCTION

Cervical cancer is the third most common type of cancer threatening women's health worldwide, with an estimated 596,800 new cases and 311,400 deaths in 2018 [1]. Cervical cancer is a carcinoma originating from the cervix, and human papillomavirus infection has been confirmed to be a major risk factor for the development of this cancer. Multiple genotypes of the human papillomavirus have been reported to be involved in the development of cervical cancer [2]. Screening programs, in combination with organized vaccination, have decreased the incidence of cervical cancer in developed countries, but a large number of cases are still reported in undeveloped areas due to the scarcity of resources and infrastructure there [3].

MicroRNAs (miRNAs/miRs) are a type of short non-coding RNA of 19-22 nucleotides in length. The genes encoding miRNAs can be located at both intergenic and intronic regions of the genome and are transcribed in an RNA polymerase II-dependent fashion. A nascent transcript known as a primary miRNA, which is characterized by a hairpin RNA structure, is recognized by Drosha, an RNase-III-like enzyme, and its cofactor DGCR8, and then processed to a 60-80 nucleotides-long precursor RNA. Subsequently, a precursor RNA is exported from the nucleus to the cytoplasm and cleaved by Dicer to release a miRNA duplex which con-

* Address correspondence to this author at the Department of Clinical Laboratory, Tianjin First Center Hospital, Tianjin, China;
E-mail: tjmuhongsci@126.com

[†]*These authors have equally contributed to the research.*

tains a guide and a passage strand. Next, a miRNA duplex is integrated into the appropriate effector complex, where it performs its biological function [4]. miRNAs participate in various types of cellular processes as critical regulators. The complex networks formed by miRNAs affect various cell processes, such as differentiation, development, and homeostasis.

Dysregulation of miRNA expression is closely associated with the development of several human diseases, including cancer [5]. The gene encoding miR-130b is located on chromosome 22 at the band 22q11.21 in human beings (Homo sapiens miR-130b gene locus, NC_000022). Significant differences in miR-130b expression levels between cancer and normal cells were widely observed in various types of tissue. Dysregulated expression of miR-130b was shown to have a notable effect on the development of cancer and cell phenotypes by affecting the expression levels of its target genes. miR-130b-3p containing extracellular vesicles promote cell proliferation, migration, and invasion of lung cancer cells but inhibit their apoptosis by suppressing the gene expression of forkhead box O3 [6]. A decrease in the miR-130b levels was observed in both prostate cancer tissues and cell lines and was correlated with an increase in proliferation, invasion, and tubule formation of human umbilical vein endothelial cells.

Conversely, overexpression of miR-130b prevented prostate cancer angiogenesis *in vitro* and *in vivo* by inhibiting the gene expression of tumor necrosis factor-α (TNF-α) [7]. The up-regulated expression of miR-130b-3p promoted angiogenesis by decreasing the gene expression levels of homeobox A5 in hepatocellular carcinoma [8]. miR-130b-3p in exosomes serves a negative role in tumorigenesis of medulloblastoma by targeting the gene encoding serine/threonine-protein kinase1, which is involved in the p53 signaling pathways [9].

Several other studies have shown that the expression of miR-130b is dysregulated in different cancer cells; however, the description of the biological functions of this miR-130 b in the growth and survival of cervical cancer cells is limited. Recently, the levels of miR-130b-5p were shown to be downregulated in cervical cancer tissues compared with benign lesions, and overexpression of miR-130b-5p suppressed colony formation and proliferation of cervical cancer cells but promoted their apoptosis [10]. In our previous study, it was also shown that gene expression levels of miR-130b were increased by TNF-α, and this protected cervical cancer cells against the toxic effects of TNF-α [11]. Herein, the expression levels of miR-130b in tissues, including normal cervical, non-cancerous precursors of cancer tissues and cancer tissues, were determined and compared in order to investigate whether miR-130b expression was dysregulated during the development of cervical cancer. As HeLa and Siha cells are representative adenocarcinomas and squamous cell carcinoma cell lines, respectively, both cell lines were used to study the functions of miR-130b in cancer cells in the present study. miR-130b levels in *in vitro* culture models of cancer cells were monitored in order to determine whether they were altered during the growth of tumor cells. The methylation levels of CpG islands close to the transcript start site (TSS) of the primary transcript of miR-130b (pri-miR-130b) were measured in cells at different growth phases, and the impact of methylation inhibitors on the expression levels of miR-130b genes was determined to examine whether the miR-130b gene was epigenetically expressed in cancer cells. The biological effects of miR-130b on cell proliferation and survival, as well as their underlying mechanisms, were explored in gain-and loss-of-function assays.

## 2. MATERIALS AND METHODS

### 2.1. Cell Culture and Plotting of Growth Curve

HeLa and Siha cells were obtained from the Key Laboratory for Critical Care Medicine of the Ministry of Health and cultured in RPMI-1640 medium supplemented with 10% (vol/vol) fetal bovine serum (HyClone, Cytiva) and 1% penicillin-streptomycin (vol/vol) (Gibco; Thermo Fisher Scientific, Inc.), and were cultured in a humidified incubator with 5% $CO_2$ at 37˚C. In total, ~$1x10^4$ cells/well were seeded in 6-well plates in triplicate and grown in a medium that was not changed over time. Both adherent and non-adherent cells were collected over the desired time periods. Cell counts were performed on a hemocytometer (Beijing Solarbio Science & Technology Co., Ltd). The average number of cells recorded at set time points in three independent experiments was used to plot the growth curves of the cancer cells. The growth phases of cells were divided into 3 sections: lag, exponential, and stationary phases. The end of the lag phase was defined by the intersection between the nearly constant cell count line at the beginning of the curve and the extrapolated exponential increase in cell count, whereas the end of the exponential phase was defined by the intersection between the increasing cell count line and the nearly constant cell number line at the end of the curve.

### 2.2. Analysis of miRNA Expression in Previously Published Datasets

The following datasets were retrieved from the Gene Expression Omnibus (GEO): GSE86100, GSE55478, GSE30656, GSE51993, and GSE19611, and were analyzed using the GEO2R online tool (ncbi.nlm.nih.gov/geo/-geo2r/?acc) with the default parameters, as described previously [12].

### 2.3. RNA Extraction

An RNA Isolation kit (Thermo Fisher Scientific, Inc.) was used for RNA extraction, according to the manufacturer's protocol. RNA concentrations were measured and determined using a NanoDrop 3300 fluorospectrometer (Thermo Fisher Scientific, Inc.).

### 2.4. Construction of Vectors

A specific primer named SCNRT was used to synthesize the cDNA encoding cyclin-dependent kinase inhibitor 1A (CDKN1A). The amplification of the coding domain of the

*CDKN1A* gene following the Kozak sequence was achieved using two pairs of primers. One pair consisted of CNF1 and CNR1, and the other of CNF2 and CNR2. The PCR products were purified and cut using restriction enzymes and then inserted into the *Kpn*I-*Xho*I cloning sites in the pcDNA3.1 control vectors to form the derived vector encoding CDKN1A proteins pcDNA3.1: *CDKN1A.* The genomic region encoding a part of the 3'untranslated region (UTR) of *CDKN1A* mRNA containing the putative miR-130b targeted site and a mutant variant encoding an RNA lacking the targeted sites were imitated using a pair of synthesized complementary DNA strands (cnutr-top and cnutr-bottom) and their derivatives (cnmut-top and cnmut-bottom), respectively. A pair of DNA strands [small-interfering RNA (si)-P21-Top and si-P21-Bottom] that were partially complementary to each other were synthesized to target the *CDKN1A* gene for RNA interference. Then the annealed DNAs of double strands were ligated into the *BamH*I-*Xho*I cloning sites downstream of the sequence encoding green fluorescent protein (GFP) in the pEGFP vector to construct a pEGFP: wt-utr and pEGFP: mut-utr vector, and into the *Bam*HI and *Hind*III restriction sites to construct a pSilencer: *CDKN1A* vector. The sequences of oligonucleotides used are listed in Table **1**.

### 2.5. Reverse Transcription-quantitative (RT-q)PCR

The cellular levels of miR-130b and their internal controls, U6 small RNA, were quantified using qPCR. cDNAs were synthesized using the miRT and U6spRT primers in the RT assays. The levels of *CDKN1A* mRNA and the internal control, β-actin, were also measured using semi-qPCR and the SCNRT and Oligod$(T)_{18}$ primers RT reactions. The amplification of cDNAs and subsequent staining of amplicons with SYBR fluorescence dye were achieved using a TB Green Premix Ex Taq kit (Takara Bio, Inc.). Measurements of stained amplicons were performed on a Roche Light cycler 480 detection system. The relative expression levels of miR-130b and *CDKN1A* mRNAs were determined using the $2^{-\Delta\Delta Cq}$ method [13]. The sequences of primers used in the experiments are provided in Table **2**. The data are presented in Supplementary Tables **1** to **4**, which are provided as proof that a 2-ΔΔCq method was used in the q PCR experiments.

**Table 1. Primers used for vector construction.**

| Name | Sequence |
|---|---|
| SCNRT | 5'-GGCGGATTAGGGCT-3' |
| CNF1 | 5'- CCGCCACCATGGCAGAACCGGCT-3' |
| CNR1 | 5'-TCCTGGCTCGTCATTAGGGCTTCCTCTTGG-3' |
| CNF2 | 5'- TGGGGTACC[a]GCCGCCACCATGG-3' |
| CNR2 | 5'-CCGCTCGAG[a]CCCTGGCTCGTCATTAG-3' |
| cnutr-top | 5'-GATCCCCCAGTTCATTGCAC[b]TTTGATTAGAC-3' |
| cnutr-bottom | 5'-TCGAGTCTAATCAAAGTGCAATGAACTGGGG-3' |
| cnmut-top | 5'-GATCCCCCAGTTCATAGGAG[b]TTTGATTAGAC-3' |
| cnmut-bottom | 5'-TCGAGTCTAATCAAACTCCTATGAACTGGGG-3' |
| si-P21-Top | 5'-GATCCGACCATGTGGACCTGTCAC[c]TTCAAGAGAGTGACAGGTCCACATGGTCTTTTTTGGAAA-3' |
| si-P21-Bottom | 5'-AGCTTTTCCAAAAAAGACCATGTGGACCTGTCACTCTCTTGAAGTGACAGGTCCACATGGTC[c]G-3' |

**Note:**[a]The nucleotide sequence above solid lines express the DNA motifs recognized by restriction enzymes. [b]The nucleotide sequence above dotted lines presented the motif encoding the region of *CDKN1A* mRNA complementary to the seed sequence of miR-130b and its derivative. [c]The nucleotide sequence above dash lines indicate the region encoding the small interfering RNA targeting *CDKN1A* mRNA. CDKN1A, cyclin-dependent kinase inhibitor 1A.

**Table 2. Primers used for semiquantitative real-time PCR.**

| Name | Sequence |
|---|---|
| Oligod$T_{18}$[a] | 5'-TTTTTTTTTTTTTTTTTT-3' |
| miRT[b] | 5'-GTCGTATCCAGTGCAGGGTCCGAGGTATTCTGCACTGGATACGACATGCCC-3' |
| U6spRT[c] | 5'-TCACGAATTTGCGTGT-3' |
| P21retF[d] | 5'-CCCGTGAGCGATGGAACTT-3' |
| P21retR[d] | 5'-CCCGTGGGAAGGTAGAGCTT-3' |
| bacRetF[e] | 5'-AGTTGCGTTACACCCTTTCTTG-3' |
| bacRetR[e] | 5'-TGTCACCTTCACCGTTCCAGT-3' |
| miRU[f] | 5'-AGTGCAGGGTCCGAGGTAT-3' |
| miRD[f] | 5'-TGCAATGATGAAAGGGCAT-3' |
| U6F[g] | 5'-CGCTTCGGCAGCACAT-3' |
| U6R[g] | 5'-ATTTGCGTGTCATCCTTGC-3' |

**Note:**[a-c]The primers were in turn used to initiate the synthesis of cDNAs encoding *CDKN1A* and *β-actin* mRNAs, miR-130bs and parts of U6 small RNAs in reverse transcription assays. [d-g]The primers were sequentially used in pairs to amplify cDNAs in PCR assays. *CDKN1A,* cyclin-dependent kinase inhibitor 1A.

### 2.6. Determination of Methylation Levels of DNA Sequences Upstream of the miR-130b Gene

The TSS of pri-miR-130b was found using the FANTOM5 web tool and shown on a UCSC (hg38) genome viewer (genome.ucsc.edu/cgi-bin/hgTracks?db =hg38&lastVirtModeType=default&lastVirtModeExtraState =&virtModeType=default&virtMode=0&nonVirtPosition=&position=chr22%3A21565713%2D21569713&hgsid=1120218429_QZUMREbGdSxow5PziSeV6J0NtJad), whereas a CpG island was identified close to the TSS using the MethPrimer software (urogene.org/cgi-bin/methprimer2/MethPrimer.cgi). Genomic DNAs were extracted using MiniBEST Universal Genomic DNA Extraction kit, following the manufacturer's instructions (Takara Bio, Inc.). The extracted DNA was treated with sodium bisulfite using the EZ DNA Methylation-Gold kit (Zymo Research Corp.). Two sets of PCR primers, UMet-F/R and Met-F/R, were used to amplify the unmethylated and methylated DNA sequences, and their sequences are listed in Table **3**. The relative levels of the methylated DNA regions near the TSS of pri-miR-130b were determined using an SYBR Green-based quantitative methylation-specific PCR, as described [14]. 5-Aza-2'-deoxycytidine (MedChemExpress) at a final concentration of 5 μM was added to the media to treat target cells 24 h prior to the extraction of the cervical cancer cell genome.

**Table 3. Primers used to determine DNA methylation levels.**

| Name | Sequence |
|---|---|
| MetF | 5'-TTATAGTAGGTTTGGCGGGG-3' (sense primer) |
| MetR | 5'-CAAAAACGCTTAAAAACCCG-3' (reverse primer) |
| UMetF | 5'-TGTTTATAGTAGGTTTGGTGGGG-3' (sense primer) |
| UMetR | 5'-AACAAAAACACTTAAAAACCCAATA-3' (reverse primer) |

### 2.7. Transfection Assays

Cervical cancer cells were transfected with exogenous nucleotides using RNA and DNA X-fect transfection reagents 96 h after cells were seeded, following the manufacturer's instructions (Takara Bio, Inc.). In brief, exogenous nucleotides were firstly mixed with X-fect RNA transfection polymer that was dissolved in X-fect Reaction Buffer by vertexing, and then the samples were incubated at room temperature to allow nanoparticle complexes to form. Subsequently, the complex solution was added to the serum-free medium. The target cells were incubated in the media containing complex solution over a 4-h time period. The depletion of the transfection complex was achieved by aspirating the media from the cells, followed by the addition of the media without a complex solution to incubate target cells over a desired time course. Of note, the serum-free medium containing transfection complex was replaced by the fresh medium at the end of the assays to determine the impact of miR-130b on cell proliferation, and by the original medium in cells that were incubated over a 96-h period, to identify the effects of miR-130b on cell survival. Cervical cancer cells were classified into different groups based on the types of transfected nucleotides: i) miR-130b (transfected with miR-130b mimic); ii) negative control (NC; transfected with negative control of miR-130b mimic); iii) inhibitor (transfected with miR-130b inhibitor); iv) inhibitor NC (transfected with the control of miR-130b inhibitor); v) pSilencer: CDKN1A (transfected with the vector knocking down the gene expression of the *CDKN1A* gene); vi) pSilencer (transfected with the pSilencer control vector); vii) miR-130b + pcDNA3.1: CDKN1A (transfected with miR-130b mimic and the vector overexpressing *CDKN1A* gene); viii) miR-130b + pcDNA3.1 (transfected with miR-130b mimic and the pcDNA3.1 control vector) ; ix) miR-130b + pEGFP (transfected with miR-130b mimic and the pEGFP control vector); x) miR-130b + pEGFP: wtUTR (transfected with miR-130b mimic and the pEGFP vector containing miR-130b-targeted site); and xi) miR-130b + pEGFP: mutUTR (transfected with miR-130b-3p mimic and the pEGFP vector containing the mutant of miR-130b-targeted site). Chemically synthesized miR-130b mimics and their negative controls were purchased from Shanghai GenePharma Co., Ltd., and the sequences of both miR-130b mimics and their negative controls are presented in Table **4**.

**Table 4. RNA oligonucleotides used in the transfection trials.**

| Name | Sequence |
|---|---|
| miR-130b mimics | 5'-CAGUGCAAUGAUGAAAGGGCAU-3'[a]<br>5'-GCCCUUUCAUCAUUGCACUGUU-3'[b] |
| NC<br>miR-130b inhibitor<br>inhibitor NC | 5'-UUCUCCGAACGUGUCACGUUUU-3'[a]<br>5'-ACGUGACACGUUCGGAGAAUUU-3'[b]<br>5'-AUGCCCUUUCAUCAUUGCACUG-3'<br>5'-CAGUACUUUUGUGUAGUACAA-3' |

**Note:**[a-b]The nucleotide sequence represent guide and passenger strands of miR-130b mimics and their controls. NC, negative control.

### 2.8. Bioinformatics Analysis of miR-130b and CDKN1A mRNA Sequence

Analysis of miR-130b (Homo sapiens microRNA miR-130b; AJ550406) and *CDKN1A* mRNA sequence (Homo sapiens *CDKN1A* mRNA; NM_000389.5) was performed using three distinct bioinformatics algorithms: TargetScan (targetscan.org/vert_72/), miRNA.org (microrna.org/microrna/home.do) and DIANA tools (diana.imis.athena-innovation.gr/DianaTools/index.php?r=tarbase/index).

### 2.9. Fluorescence Analysis

Following seeding on a 24-well plate at a density of $2.5x10^4$ cells per well, cells were incubated overnight and transfected the following day. The proteins were extracted from cells 48 h after transfection using a mammalian cell extraction kit, following the manufacturer's instructions (APExBIO). The obtained supernatants containing fluorescence proteins were transferred into the wells of a 96-well plate. The intensities of fluorescence of GFP and red fluorescent protein were measured using an EnSpire™ Multilabel Reader (PerkinElmer, Inc.). Each group consisted of three independent assays.

### 2.10. Cell Counting Kit-8 (CCK-8) Assays

Cells were seeded into a 96-well plate at a density of 100 cells per well. The transfections were performed 96 h after

cells were seeded. Serum-free media containing transfection complex was replaced by fresh or original medium, as required. The cell culture was supplemented with a CCK-8 commercial stock solution (Wuhan Boster Biological Technology, Ltd.) at the appropriate time points, and the cells were incubated at 37°C for 1 h. The optical density was measured at 450 nm on an EnSpire™ Multilabel Reader (PerkinElmer, Inc.), with three independent assays per group.

### 2.11. Determination of Cell Cycle Distribution

Cell cycle distribution assays were performed as follows: $1x10^6$ cells were incubated in 70% ethanol at 4˚C for 4 h and then incubated in staining buffer including propidium iodide (PI) in the dark at room temperature for >30 min. The distribution of cell cycle phases was analyzed and presented using ModFit *LT*™ Version 4.0 (Verity Software House Inc.) following flow cytometry analysis using a FACSCalibur system (BD Biosciences).

### 2.12. Measurement of DNA Synthesis Rates

HeLa and Siha cells, at a density of $2x10^5$ cells/well, were seeded and cultured in the 6-well plates overnight. Transfections were performed the following day. Target cells were cultured over the desired time periods. The DNA synthesis rates were measured using an EdU Apollo488 In Vitro Flow Cytometry kit, following the manufacturer's instructions (Guangzhou RiboBio, Co., Ltd.).

### 2.13. Western Blotting

Western blotting was performed as previously described [11]. Briefly, RIPA buffer (Beijing Solarbio Science & Technology Co., Ltd.) was used to lyse cancer cells. A total of 30 μg protein was mixed with loading buffer, loaded in each lane on an SDS-gel, and resolved using SDS/PAGE. After proteins were transferred to PVDF membranes, the membrane was blocked in TBS-Tween (TBST) buffer containing non-fat milk. Next, the membranes were incubated with a rabbit anti-human polyclonal antibody against CDKN1A (1:500; ProteinTech Group, Inc.) or an anti-GADPH antibody (1:200; Tianjin SaierBio Technology, Inc.). The antibodies that were not bound to their target proteins were washed off from the membrane using TBST buffer. The membrane was then incubated in fresh blocking buffer with a horseradish peroxidase-conjugated goat anti-rabbit polyclonal antibody IgG (H+L) antibody (1:2,000; ProteinTech Group, Inc.) and washed with TBST buffer. Signals were visualized using an enhanced chemiluminescence detection kit (Wuhan Boster Biological Technology, Ltd.), and the relative levels of CDKN1A protein were analyzed and determined using AlphaView SA software (ProteinSimple).

### 2.14. Comet Assays

Comet assays were performed as described previously [15]. Briefly, ~$8x10^3$ cells were used alongside agarose at a low melting temperature. Cells were placed on the surface of a slide pre-coated with agarose. Staining of the slides was performed in a solution containing propidium iodide after electrophoresis, followed by rinsing in distilled water. The DNA olive tail moments (OTMs) in 50 comet images captured from each slide were determined using the Comet Assay Software Project imaging software as previously described [16].

### 2.15. Measurement of γ-H2AX Levels

γ-H2AX levels were determined as previously described [17]. Briefly, target cells were fixed in 70% ethanol over a 4-h period at 4˚C, following fixing in formaldehyde solution on ice. Cells were washed with PBS buffer and 1% BSA solution and then immersed in 100 μl 1% BSA reagent. The primary antibody (1:100; Abcam) against γ-H2AX (phospho S139) protein and the Alexa Fluor® 488-conjugated secondary antibody (1:100; Abcam) were used for the detection of γ-H2AX protein expression. The fluorescence in the dye was excited and detected on a BD Accuri C6 Plus System (BD Biosciences).

### 2.16. Measurement of Apoptotic Rates

Phosphatidyl-serine on the surface of cell membranes and intracellular DNAs was recognized and labelled using an Annexin-V apoptosis kit (BD Biosciences). The percentages of apoptotic cells were determined on a BD Accuri C6 Plus System (BD Biosciences).

### 2.17. Statistical Analysis

Analysis of the experimental data was performed using GraphPad Prism version 5.0 (GraphPad Software, Inc.). Numerical data are presented as the mean ± the standard error (S.E.) of the mean. Where relative values were used, the means of the data obtained from the control groups were defined as 1 or 100%, and the data from the experimental groups were normalized against the control. A Student's two-tailed unpaired or paired *T*-test was used to compare differences between two groups. A one-way analysis of variance (ANOVA), followed by a post hoc Dunnett's test or Bonferroni's corrections, was used to compare the differences between multiple groups. $P < 0.05$ was considered to indicate a statistically significant difference.

## 3. RESULTS

### 3.1. Dynamic Changes in miR-130b Expression Levels are Associated with the Alterations in the Methylation Levels of a CpG Island Close to the TSS of pri-miR-130b

It was shown that the expression levels of miR-130b were increased in both squamous cell carcinoma and adenocarcinoma tissues when compared with the corresponding levels in normal controls. However, there was no significant difference in the miR-130b levels between the cervical intraepithelial neoplasia tissues and the normal samples (Table **5**). Following the conversion of miR-130b absolute counts into relative values, in which the average levels of miR-130b expressed in normal tissues acted as the reference points, the analysis of the relative values derived from the

**Table 5. Expression levels of miR-130b deposited in databases associated with CIN and cervical carcinoma.**

| Repository | Type of Tissue Used | ($Log_2$) Fold Change | *P*-value | Dysregulation |
|---|---|---|---|---|
| GSE86100 | SCC *vs.* Normal | 2.067 | 0.023 | Up |
| GSE55478 | ADC *vs.* Normal | 1.802 | 0.038 | Up |
| GSE30656 | SCC *vs.* Normal | 0.483 | 0.020 | Up |
| - | ADC *vs.* Normal | 0.356 | 0.034 | Up |
| - | CIN II-III stage *vs.* Normal | 0.130 | 0.172 | NS[d] |
| GSE51993 | CIN I stage *vs.* Normal | -1.563 | 0.793 | NS |
| - | CIN III stage *vs.* Normal | -0.128 | 0.973 | NS |
| GSE19611 | LSIL *vs.* Normal | -0.065 | 0.465 | NS |
| - | HSIL *vs.* Normal | -0.133 | 0.926 | NS |

**Abbreviations:** SSC, squamous cell carcinoma; ADC, adenocarcinoma; CIN, cervical intraepithelial neoplasia; NS, no significance; LSIL, low-grade intraepithelial lesions; HSIL, high-grade intraepithelial lesions.

GSE86100 and GSE30565 datasets showed that the miR-130b levels in squamous cell carcinoma tissues increased by 0.65- and 0.42-fold and those derived from the GSE54478 and GSE30565 datasets showed that the miR-130b levels increased by 0.43- and 0.31-fold in adenocarcinoma tissues compared with the normal cervical tissue (Fig. **1A**). The initial 48-h period after the cells were seeded was defined as a lag phase of cell growth, during which the number of cells grew slowly. The 48-120 h period was considered the exponential phase, during which the cells divided rapidly. The stationary phase started 120 h after target cells were seeded and lasted for 24 h. The length of the exponential phase was extended to up to 144h rather than 120 h when the original medium was replaced by a fresh medium 96 h after cells were seeded (Fig. **1B**). The transcription levels of a gene were expected to be dynamic in the cells in response to external and internal stimuli during cell growth, as the environment surrounding the cells was changing. The miR-130b levels were measured during the lag, exponential, and stationary phases. Compared with the levels measured during the lag phase, 48 h after HeLa and Siha cells were seeded, the relative levels of miR-130b increased by 0.45- and 0.32-fold, respectively, during the exponential phase when target cells were incubated in medium for 96 h, but reduced by 36.02 and 18.01% during the stationary phase when target cells were cultured over a 144 h time period, respectively (Fig. **1C**). The nucleotide at position 21,652,184, which is 1,121 nucleotides away from the 5'end of the region encoding pre-miR-130b on chromosome 22, was identified as the TSS of pri-miR-130b, and the sequence located at position 21,651,791-21,652,759 was recognized as a prominent CpG island upstream of the DNA region encoding the miR-130b gene (Fig. **S1**). The percentages of these methylated CpG islands increased by 4.31- and 2.06-fold in the HeLa and Siha cells, respectively, during the stationary phase, when compared with the exponential phase (Fig. **1D**). When compared with DMSO, 5-Aza-2'-deoxycytidine reduced the percentage of methylated CpG islands by 70.68 and 41.00% in HeLa and Siha cells, respectively, during the stationary phase and increased the expression levels of miR-130b by 5.22- and 4.55-fold (Fig. **1E** and **F**).

### 3.2. Gene Expression of CDKN1A mRNA is Negatively Regulated by miR-130b

Bioinformatics analysis showed that the sequence located at positions 1,146-1,152 of the 3'UTR in *CDKN1A* mRNA was complementary to the seed region of miR-130b (Fig. **2A**). The miR-130b levels in the HeLa and Siha cells were first determined 24 h after transfection to confirm that miR-130b mimics or their inhibitors had been successfully transfected into the HeLa and Siha cells. The miR-130b levels were increased in the target cells transfected with miR-130b mimics and reduced in the cells with miR-130b inhibitors when compared with their respective negative controls (Fig. **S2**). Compared with NCs, miR-130b mimics caused a 27.86 and 15.52% reduction in the intensity of fluorescence emitted from HeLa and Siha cells, respectively, containing pEGFP: wt-utr vectors, but no significant changes were observed in the intensity from the target cells containing pEGFP: mut-utr vectors (Fig. **2B**). 42.21 and 27.59% decrease were observed in the mRNA expression levels of *CDKN1A* in HeLa and Siha cells transfected with miR-130b mimics, compared with the corresponding levels in the target cells transfected with the NCs (Fig. **2C**). In agreement with this decrease in the levels of *CDKN1A* mRNA, the protein levels of *CDKN1A* were reduced by 57.55 and 20.55% in miR-130b-transfected HeLa and Siha cells when compared with the NC-transfected cells (Fig. **2D**).

### 3.3. miR-130b Increases Cell Viability and Promotes Both DNA Synthesis and the Transition from the G1 to the S Cycle phase of Cells During the Exponential Growth Phase by Reducing the *CDKN1A* Gene Expression

Both the *CDKN1A* mRNA and protein levels were first assessed in the HeLa and Siha cells, transfected with pSilencer: *CDKN1A* or pcDNA 3.1: *CDKN1A* 24 h after transfection. *CDKN1A* mRNA and protein levels were decreased in the cells transfected with pSilencer: *CDKN1A*, and they were increased in the cells transfected with the pcDNA3.1: *CDKN1A* when compared with their respective empty vector controls (Fig. **S3A** and **B**). Compared with their respective negative controls, miR-130b mimics increased the viability of HeLa and Siha cells in the extended exponential phases,

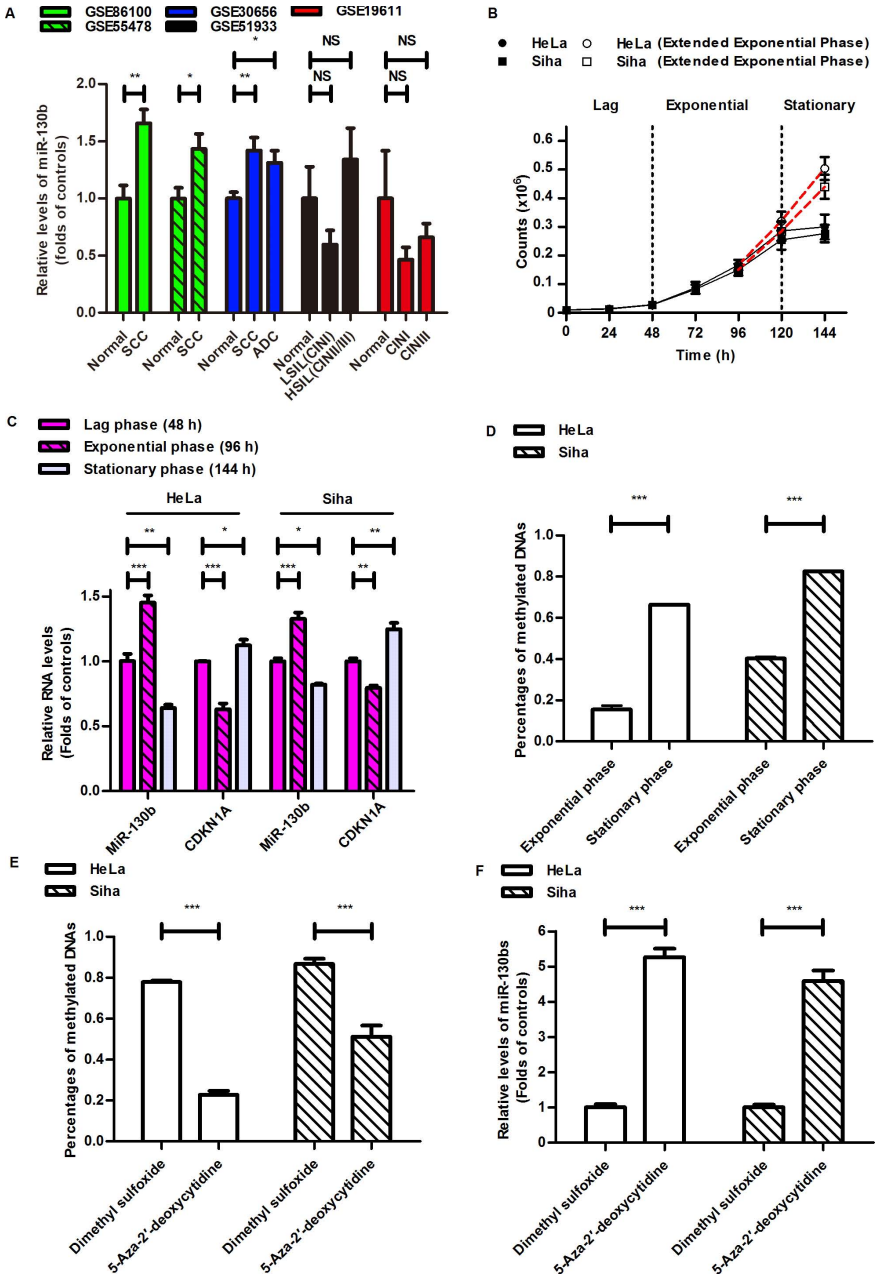


**Fig. (1).** miR-130b expression levels in tissues and cell lines. (**A**) Relative expression levels of miR-130bs in CINs, SCCs, ADCs, and normal cervixes. Green, shadow green, blue, black, and red columns sequentially presented the relative levels of miR-130bs, into which primary data retrieved from GSE86100, GSE55478, GSE30656, GSE51933, and GSE19611 were converted. (**B**) Growth curves of HeLa and Siha cells. A solid graph drawn in black depicts changes in the number of cells progressing through a series of growth phases, including the lag, exponential and stationary phases, while dash curves plotted in red describe varieties of cell counts at extended exponential phases. The full symbols indicated the counts of cells that grew in media not changed over a 144h- time period, while the empty ones indicated the numbers of cells that were incubated in media aspirated and replaced by the fresh ones 96h after the target cells were seeded. (**C**) The relative expression levels of miR-130bs were measured at indicated time points in HeLa and Siha cells. Purple, shadow purple, and gray columns, respectively, indicated the relative levels of miR-130bs or *CDKN1A* mRNAs determined 48, 96, and 144 h after HeLa and Siha cells were planted. (**D**) Percentage of methylated CpG islands close to the TSSs of pri-miR-130bs in cervical cancer cells at different growth phases. (**E**) Effect of 5-Aza-2'-deoxycytidine administration on the methylation of CpG islands near the TSSs of pri-miR-130b in cervical cancer cells at stationary phases of growth. (**F**) Impact of 5-aza-2'-deoxycytidine administration on the gene expression levels of miR-130bs in cervical cancer cells at stationary phases of growth. Blank and shadow columns indicate the percentages of CpG islands in HeLa and Siha cells, respectively. Data are described as the mean ± S.E. ($n$=3). The bars indicate the deviations from the mean. **P*<0.05; ***P*<0.005; ****P*<0.001; **Abbreviations**: SSC, squamous cell carcinoma; ADC, adenocarcinoma; CIN, cervical intraepithelial neoplasia; N.S., non-significant (*A higher resolution / colour version of this figure is available in the electronic copy of the article*).

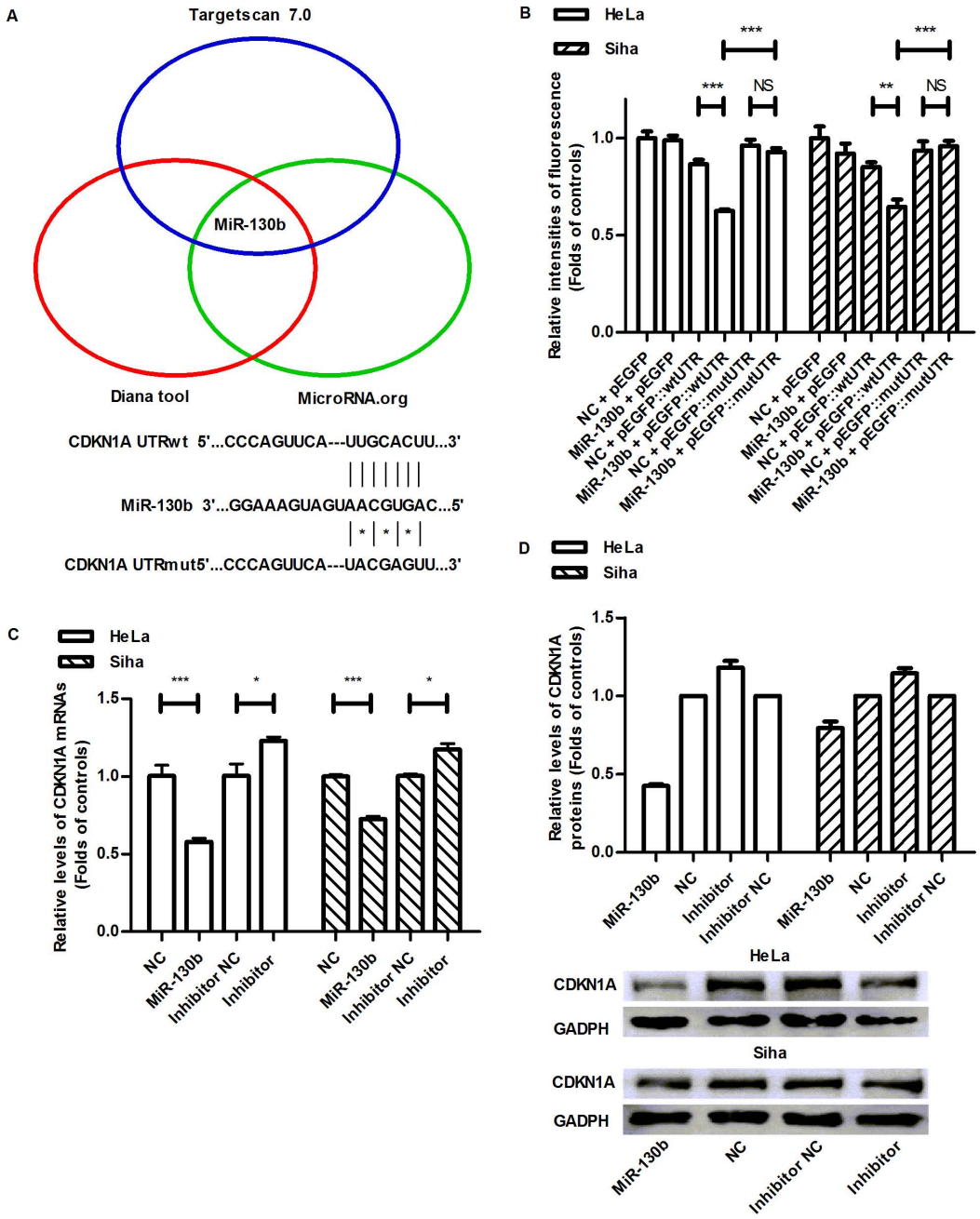


**Fig. (2).** miR-130b-regulated gene expression of *CDKN1A*. (**A**) Putative miR-130b-targeted site presented in the 3'UTR of *CDKN1A* mRNA. Three circles of different colors in the Ven diagram respectively represent a different assembly of miRNAs, which were predicted to target *CDKN1A* mRNAs using three distinct bioinformatics algorithms involving TargetScan, miRNA.org, and DIANA tools. miR-130b presented in the overlapped region of three circles indicated that miR-130b was predicted to target *CDKN1A* mRNAs using all the algorithms. Dotted lines represent DNA sequences not shown in the figure. The base pairs were indicated as vertical lines. Mutated points in miR-130b-targeted sites are indicated by the words marked with stars. (**B**) Effects of miR-130bs on gene expression levels of *GFPs* encoded by mRNAs with or without regions complementary to the seed sequences of miR-130bs. The relative fluorescence intensities of GFPs in HeLa and Siha cells are respectively presented using blank and shadow columns. (**C**) Impact of miR-130bs on the expression levels of *CDKN1A* mRNAs in HeLa and Siha cells. The relative levels of *CDKN1A* mRNAs in HeLa and Siha cells are sequentially presented as blank and shadow columns. (**D**) Effects of miR-130bs on the protein levels of GFPs in HeLa and Siha cells. Graphic data obtained by western blotting are provided at the bottom of the corresponding statistical analyses. The relative levels of CDKN1A proteins in HeLa and Siha cells are sequentially presented as blank and shadow columns. Data are presented as the mean ± S.E. ($n$=3). The bars indicate the deviations from the mean. *$P$<0.05; **$P$<0.005; ***$P$<0.001; **Abbreviations**: CDKN1A, cyclin-dependent kinase inhibitor 1A; UTR, untranslated region; GFP, green fluorescent protein; N.S., non-significant (*A higher resolution / colour version of this figure is available in the electronic copy of the article*).

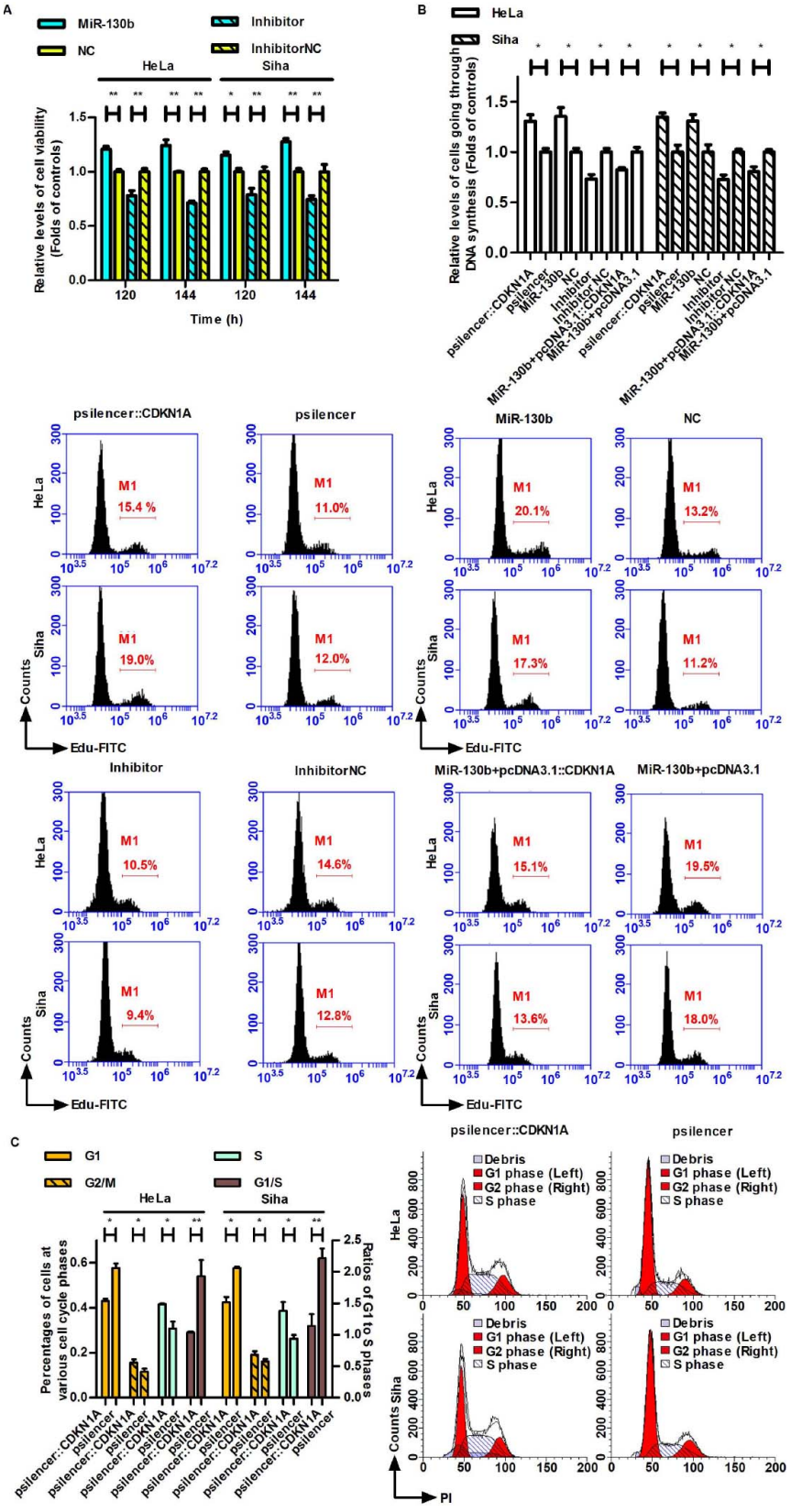
A
MiR-130b
NC
Inhibitor
InhibitorNC
HeLa
Siha
Relative levels of cell viability (Folds of controls)
Time (h)
B
HeLa
Siha
Relative levels of cells going through DNA synthesis (Folds of controls)
psilencer::CDKN1A
psilencer
MiR-130b
NC
Inhibitor
InhibitorNC
MiR-130b+pcDNA3.1::CDKN1A
MiR-130b+pcDNA3.1
M1
15.4 %
11.0%
20.1%
13.2%
19.0%
12.0%
17.3%
11.2%
10.5%
14.6%
15.1%
19.5%
9.4%
12.8%
13.6%
18.0%
Counts
Edu-FITC
C
G1
S
G2/M
G1/S
Percentages of cells at various cell cycle phases
Ratios of G1 to S phases
Debris
G1 phase (Left)
G2 phase (Right)
S phase
Counts Siha
PI

**Fig. (3) cont....**

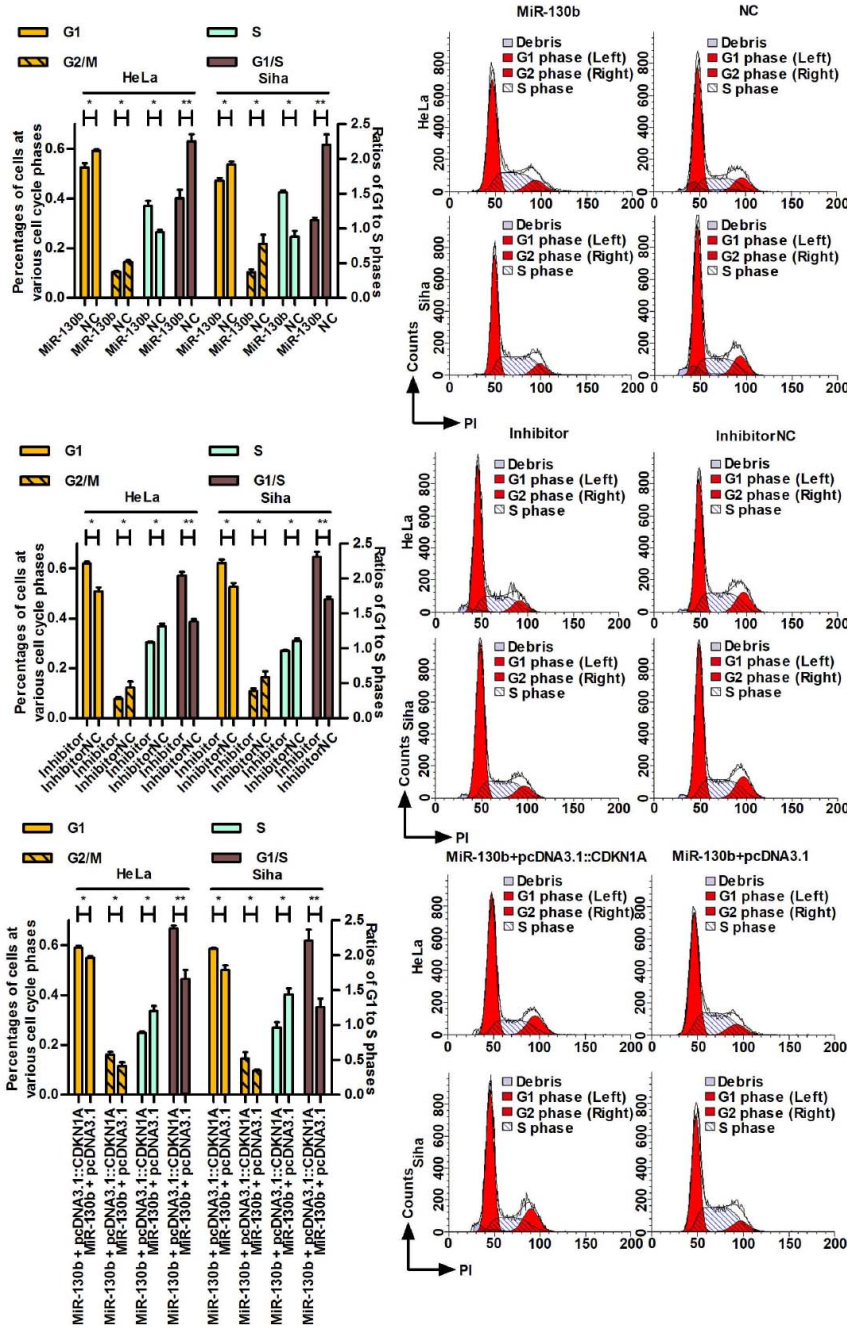


**Fig. (3).** Impact of miR-130bs on viability, DNA synthesis, and distribution of cell cycle phases of cells at exponential phases. (**A**) Impact of miR-130bs on viability at extended exponential phases. Cyan and yellow columns without shadows indicate the viability of HeLa and Siha cells, respectively, which were transfected with miR-130b mimics or their NCs 120 or 144 h after cells were planted. The columns with shadows indicate the viability of cells transfected with inhibitors or their NCs. (**B**) Impact of both miR-130bs and CDKN1A proteins on DNA synthesis rates. Blank and shadow columns represented the relative levels of HeLa and Siha cells, respectively, which were transfected with indicated oligonucleotides and/or plasmids and experienced DNA synthesis 144 h after target cells were seeded. (**C**) Impact of both miR-130bs and CDKN1A proteins on the distribution of cell cycle phases. Orange, shadow orange, and light-cyan columns subsequentially expressed percentages of cells that were transfected with indicated oligonucleotides and/or plasmids 144 h after target cells were planted. Brown columns indicated the ratio of G1 to S cell cycle phases. Gray, red, and shadow areas subsequentially indicated cell debris, G1, G2, and S cell cycle phases. Representative graphic data have been provided at the bottom or on the right sides of the statistical analysis of the graphic data. Data are presented as mean ± S.E. ($n$=3). The bars indicate the deviations from the mean. *$P$<0.05; **$P$<0.005; **Abbreviations**: NCs, negative controls; CDKN1A, cyclin-dependent kinase inhibitor 1A; N.S., non-significant (*A higher resolution / colour version of this figure is available in the electronic copy of the article*).

and the inhibitors reduced cell viability (Fig. **3A**). The EdU Apollo488 *In Vitro* Flow Cytometry kit was used to determine the percentage of cells undergoing DNA synthesis. The percentage of the right peaks indicates the proportion of cells in which DNA is replicated. The increase in the percentage of the right peak indicates the increased proportion of the cells in which DNA is synthesized. The percentage of HeLa and Siha cells undergoing DNA synthesis increased by 1.30- and 1.35-fold following transfection of pSilencer: *CDKN1A* and increased by 1.35- and 1.31-fold after the target cells were transfected with miR-130b mimics, compared with their corresponding controls. When compared with inhibitor NCs, inhibitors reduced the percentage of HeLa and Siha cells in which DNA was replicating by 26.59 and 27.11%. Compared with the pcDNA3.1 control vector, transfection of pcDNA3.1: *CDKN1A* resulted in a reduction in the proportion of miR-130b-transfected HeLa and Siha cells that were synthesizing DNAs by 17.64 and 19.50%, respectively (Fig. **3B**). Following its transfer into the target cells, pSilencer: *CDKN1A* decreased the ratio of cells in the G1 to S phases by 46.23 and 48.55%, respectively, compared with the pSilencer empty vector. miR-130b mimics decreased the ratio by 36.37 and 49.50% in HeLa and Siha cells, respectively, compared with the NCs. Compared with the inhibitor NCs, transfection of the inhibitors resulted in a 1.48- and 1.36-fold increase in the ratio of cells in the G1 to S phase of the cell cycle in HeLa and Siha cells, respectively. A 1.44- and 1.75-fold increase in the proportion of cells in the G1 to S phase was observed in the HeLa and Siha cells, respectively, transfected with pcDNA3.1: *CDKN1A* + miR-130b mimics, compared with the pcDNA3.1 control + mimic transfected cells (Fig. **3C**).

### 3.4. miR-130b-mediated Inhibition of CDKN1A Gene Expression Reduces Cell Viability, Increases DNA Damage, and Increases Apoptosis of Cells During the Stationary Phase

It was noted that the expression levels of the miR-130b gene were decreased in the cells during the stationary phase when compared with those during the lag phase. Thus, miR-130b mimics were transfected into the target cells to determine whether restoration of the miR-130b levels affected cell survival during the stationary phase. The results showed that the viability of target cells during the stationary phase was significantly reduced by miR-130b mimics, compared with the NCs (Fig. **4A**). It was hypothesized that miR-130b induced the death of cells at the stationary phase. This presumption was confirmed by the increase in the activity of lactic dehydrogenase and aspartate aminotransferase in the culture supernatants, which was measured following the manual presented in Appendix S1/cell count ratio, as well as the miR-130b-induced increase in the apoptotic rates of target cells during the stationary phase (Fig. **S4** and **4B**). However, there was no significant increase in the viability of cells when they were transfected with miR-130b inhibitors. Blocking miR-130b function did not have a notable effect on the viability of cells during the stationary phase, but increasing miR-130b gene expression did. Therefore, inhibitors were not used in the other assays, which were performed to explore the roles of miR-130b on the survival of the target cells during the stationary phase. The increase in OTMs due to gene silencing of *CDKN1A*, induced by transfection of either pSilencer: *CDKN1A* or miR-130b mimics into target cells was observed. The mean levels of DNA OTMs in HeLa and Siha cells transfected with pSilencer: *CDKN1A* vectors were increased by 1.82- and 2.02-fold, as compared with the corresponding levels in cells transfected with the pSilencer control. The miR-130b mimics delivered into HeLa and Siha cells caused a 2.11- and 1.77-fold increase in the mean levels of OTMs in target cells when compared with the NCs, whereas the pcDNA3.1: *CDKN1A* vector decreased OTM levels by 64.55 and 64.81%, compared with the pcDNA3.1 controls in HeLa and Siha cells, respectively, containing miR-130b mimics (Fig. **4B**). The levels of phosphorylated H2AX termed γ-H2AX have been shown to be positively correlated with the count of DNA double-strand breaks (DSBs) and have been widely used as a marker of DSBs in several experimental studies [17]. pSilencer: *CDKN1A* vectors, as compared with pSilencer, increased the mean levels of γ-H2AX proteins by 2.14- and 2.03-fold in HeLa and Siha cells, respectively. As compared with the NCs, miR-130b mimics resulted in a 2.66- and 2.28-fold increase in the protein levels of γ-H2AX protein in HeLa and Siha cells, respectively, whereas the pcDNA3.1: *CDKN1A* vector, which was transfected along with miR-130b mimics, decreased γ-H2AX levels by 48.28 and 47.66% in HeLa and Siha cells, respectively, when compared with the pcDNA3.1 vector-transfected cells (Fig. **4C**). As shown, the increases in the count of γ-H2AX proteins as markers of DSBs were observed in cells that suffered from alterations of *CDKN1A* gene expression, whereas the enhanced gene expression of *CDKN1A* decreased the levels of γ-H2AX proteins in cells transfected with miR-130b mimics. When compared with the controls, the pSilencer: *CDKN1A* vector resulted in a 1.86- and 2.10-fold increase in the rates of apoptosis of HeLa and Siha cells, respectively. Compared with the NCs, miR-130b mimics resulted in a 1.64- and 1.93-fold increase in the proportion of apoptotic HeLa and Siha cells. Compared with the control vectors, the transfection of pcDNA3.1: *CDKN1A* vectors in combination with miR-130b mimics yielded a 37.20 and 41.75% decrease in the percentage of HeLa and Siha cells undergoing apoptosis, respectively (Fig. **4D**).

## 4. DISCUSSION

Based on the analysis of data retrieved from GEO, the expression levels of miR-130b were found to be increased in both squamous cell carcinoma and adenocarcinoma, but not in cervical intraepithelial neoplasia, when compared with the levels in normal cervical tissue adjacent to the lesions (Fig. **1A**). These findings indicated that miR-130b was upregulated specifically in tumors and suggested that miR-130b may serve a critical role in the development of cervical cancer. The cellular levels of miR-130b, which were determined at the desired time points within the lag, exponential and stationary phases of cell growth, were found

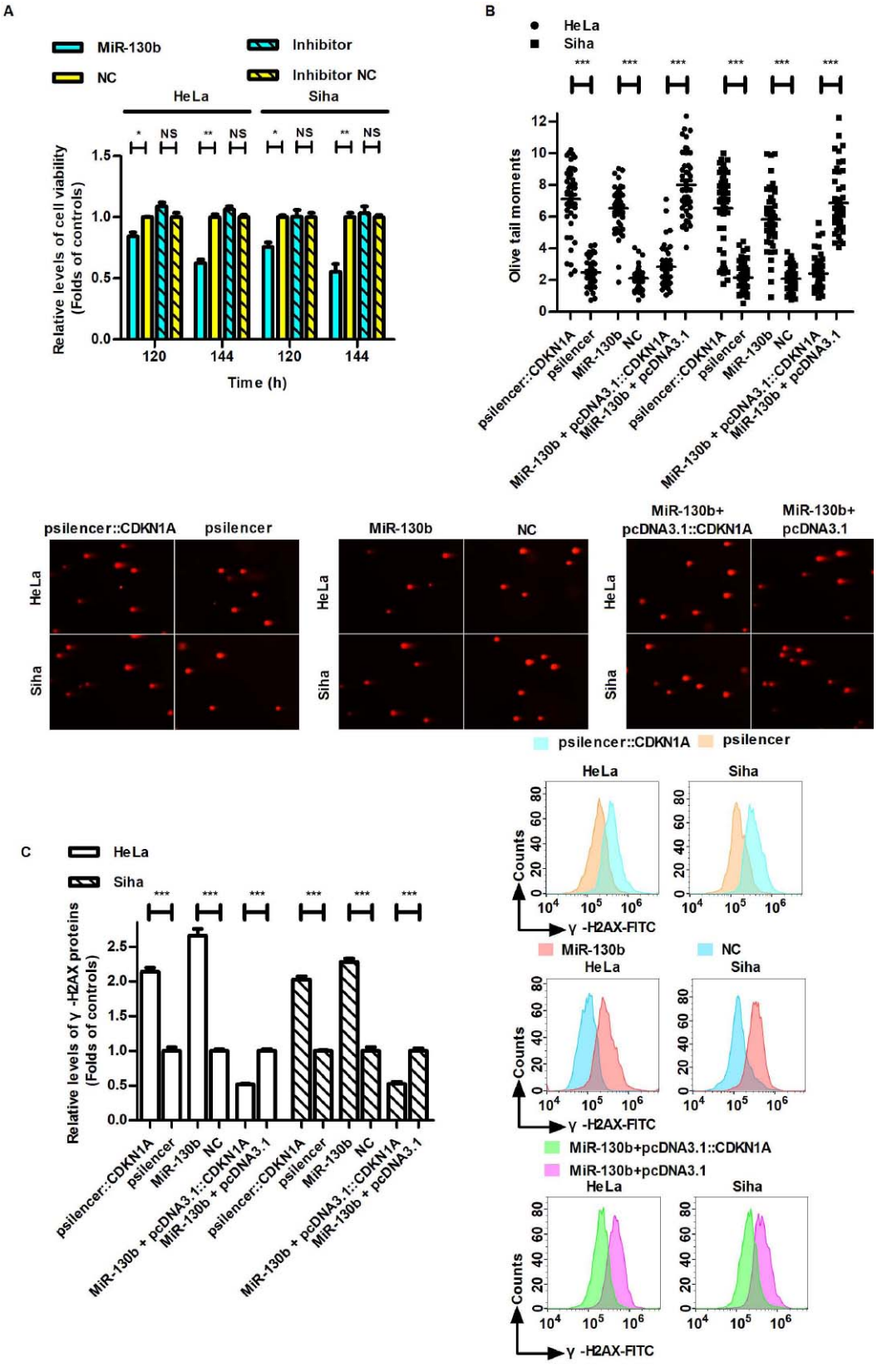
A
MiR-130b
NC
Inhibitor
Inhibitor NC
HeLa
Siha
Relative levels of cell viability (Folds of controls)
Time (h)
B
HeLa
Siha
Olive tail moments
psilencer::CDKN1A
psilencer
MiR-130b
NC
MiR-130b + pcDNA3.1::CDKN1A
MiR-130b + pcDNA3.1
C
Relative levels of γ -H2AX proteins (Folds of controls)
γ -H2AX-FITC
Counts
MiR-130b+pcDNA3.1::CDKN1A
MiR-130b+pcDNA3.1

**Fig. (4) cont....**

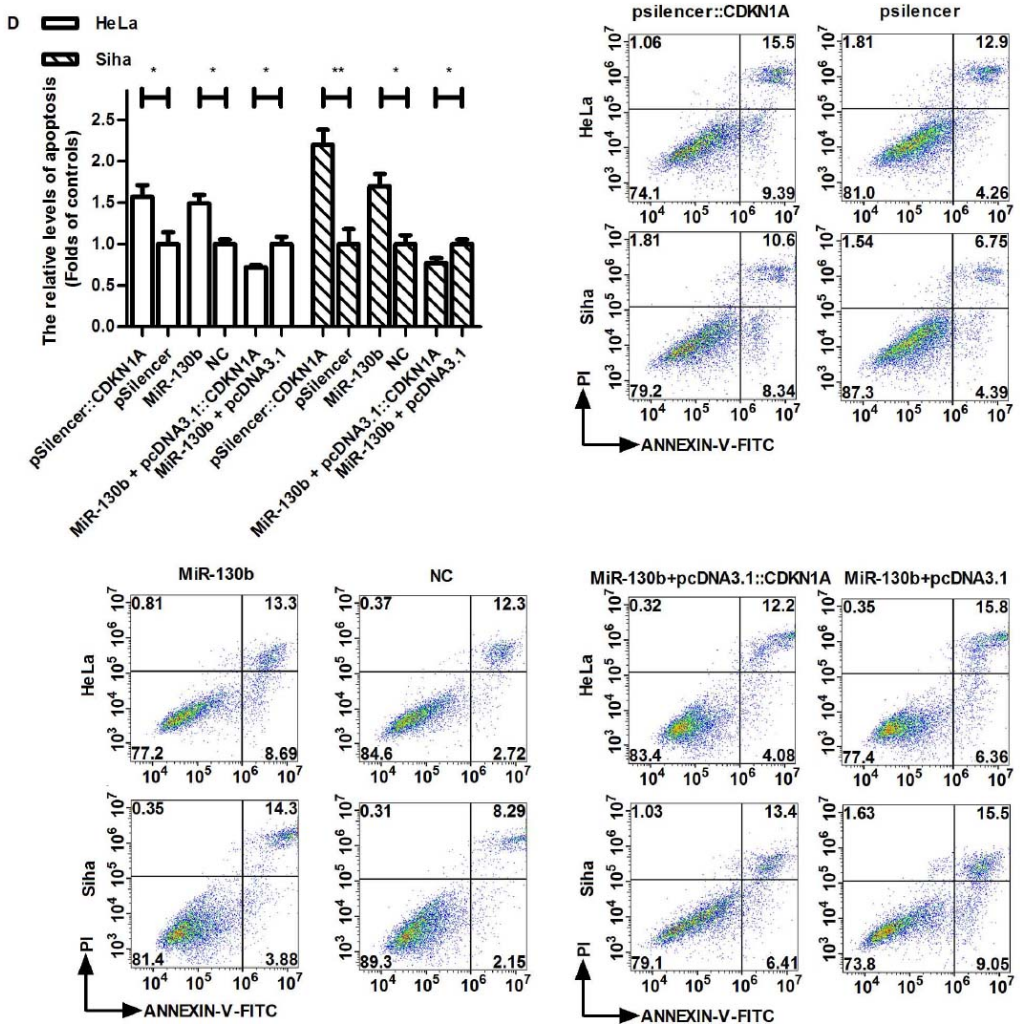


**Fig. (4).** Effects of miR-130bs on viability, DNA breaks, and cell apoptosis of the cells at stationary phases. (**A**) Effects of miR-130bs on the viability of cells at stationary phases. Cyan and yellow columns without shadows indicate the viability of HeLa and Siha cells, respectively, which were transfected with miR-130b mimics or their NCs 120 or 144 h after cells were planted. The columns with shadows indicate the viability of cells transfected with inhibitors or their NCs. (**B**) Impact of miR-130bs and CDKN1A proteins on OTMs. The target molecules of red fluorescent were the DNA molecules stained by the ethidium bromide. Circles and squares separately express the OTMs in HeLa and Siha cells, respectively, transfected with indicated oligonucleotides and/or plasmids 120 h after target cells were planted. (**C**) Effects of miR-130bs and CDKN1A proteins on the relative levels of γ-H2AX proteins. Blank and shadow columns, respectively, indicate the relative levels of H2AX proteins in HeLa and Siha cells transfected with the indicated oligonucleotides and/or plasmids120 h after target cells were seeded. (**D**) Impact of miR-130bs and CDKN1A proteins on apoptotic rates. Blank and shadow columns indicate the relative levels of apoptosis of HeLa and Siha cells, respectively, transfected with the indicated oligonucleotides and/or plasmids120 h after target cells were seeded. Representative graphic data have been provided on the right side or at the bottom of their statistical analysis. Data are described as the mean ± S.E. ($n$=3). The bars indicate the deviations from mean. *$P$<0.05; **$P$<0.005; NCs, negative controls; CDKN1A, cyclin-dependent kinase inhibitor 1A; N.S., non-significant. (*A higher resolution / colour version of this figure is available in the electronic copy of the article*).

to be significantly different. As compared with the levels measured during the lag phase, the relative levels of miR-130b determined during the exponential phase increased, whereas the levels during the stationary phases decreased (Fig. **1C**). The methylation levels of an identified CpG island near the TSS of pri-miR-130b were measured in the target cells during the different growth phases to investigate whether there was a connection between the methylation of the CpG island and the gene expression of miR-130b. The high levels of miR-130b paralleled the low percentages of methylated CpG islands in target cells during the exponential phase, and similarly, at the stationary phase, the methylation levels were high, explaining the low expression of miR-130b. In addition, methylation inhibition increased the expression of the miR-130b gene (Fig. **1E** and **F**). Therefore, methylation of the CpG islands was suggested to control the expression of the miR-130b gene in cervical cancer cells.

A potential miR-130b-targeted site in the 3'UTR of *CDKN1A* mRNA was identified in the present study (Fig. **2A**). In order to investigate whether the putative targeted site mediated miR-130b-regulated gene expression of *CDKN1A*, DNA fragments encoding RNA containing the targeted site were integrated into a fluorescence-based reporter gene vector downstream of the protein-encoding domain of the *GFP* gene. A reduction in the fluorescence intensity reflected a decrease in the gene expression levels of *GFP*. miR-130b mimics resulted in a reduction in the expression levels of *GFP* genes when co-tranfected with the pEGFP: wtUTR vectors, but no significant changes were observed in the levels of *GFP* in either the pEGFP or pEGFP: mutUTR plasmids when compared with the respective NCs (Fig. **2B**). These data, obtained from a combination of in silico analysis and fluorescence assays, demonstrated that miR-130b could inhibit the expression of a target gene by binding the sequence which imitated the target site complementary to the seed region of miR-130b. The decrease in *CDKN1A* mRNA levels showed that miR-130b could stimulate the degradation of *CDKN1A* mRNAs, and this led to a reduction in the protein levels of CDKN1A alone or accompanied by inhibition of protein translation (Fig. **2C** and **D**). The levels of *CDKN1A* mRNAs in the cells at different growth phases were also determined to assess whether there was a negative relationship between the expression levels of miR-130b and the mRNA *CDKN1A* levels alongside the growth of the cervical cancer cells. The mRNA expression levels of *CDKN1A* in the exponential phases were reduced compared with that during the lag phase, whereas the corresponding levels in the cells during the stationary phase increased (Fig. **1C**).

An inhibitor-induced decrease in the viability of target cells during the extended exponential phase showed that miR-130b might promote the proliferation of cells at the exponential phase. This hypothesis was further supported by the fact that a miR-130b-induced increase in cell viability was also observed (Fig. **3A**). In addition, the cancer cell counts were clearly increased by miR-130b mimics compared with the NCs (Fig. **S3C**). A proliferating cell nuclear antigen (PCNA) recruits a pol-δ to ensure the elongation of a continuous leading strand and discontinuous lagging strand in the process of DNA replication [18]. The CDKN1A protein has a negative effect on DNA synthesis by directly binding to PCNA [19]. In accordance with the above description, knocking down the gene expression of *CDKN1A* accelerated the rate of DNA synthesis, which was shown as an increase in the percentage of cells undergoing DNA synthesis. Since it was shown that miR-130b was able to suppress the gene expression of *CDKN1A*, it is reasonable to assume that the count of cells undergoing DNA synthesis was increased by miR-130b. Furthermore, the restoration of the number of cells undergoing DNA synthesis caused by the overexpression of the *CDKN1A* gene in the target cells containing miR-130b mimics showed that the miR-130b-induced reduction in the expression levels of the *CDKN1A* gene was responsible for the acceleration of the DNA synthesis rate (Fig. **3B**). Besides taking part in blocking the synthesis of DNA, the CDKN1A protein acts as a cell cycle inhibitor by inhibiting the activity of cyclin-CDK complexes [20]. In agreement with this established role, downregulation of *CDKN1A* gene expression, as a result of both transfection of pSilencer: *CDKN1A* vectors and miR-130b mimics into target cells, decreased the ratio of cells at the G1 cell cycle phase to those at the S phase. Overexpression of CDKN1A in miR-130b-transfected cells decreased the proportion of cells undergoing transition from the G1 phase to the S phase (Fig. **3C**). These data indicated that miR-130b promoted cell cycle progression to the S phase through its inhibition of the expression of the*CDKN1A* gene. It has been previously shown that the CDKN1A protein is involved in different DNA repair processes due to its interaction with DNA repair proteins [21]. Considering that DNA double-strand breaks (DSBs) are the most biologically hazardous type of DNA damage to a cell [22], the count of DSBs was determined in the present study. As shown in Fig. (**4C**), the results suggested that the miR-130b-induced downregulation of the *CDKN1A* gene resulted in the accumulation of DSBs. CDKN1A proteins are involved in DSB repair by binding to PCNA proteins when they are recruited to initiate the DNA synthesis associated with recombination [23]. A reduction in the CDKN1A protein levels may negatively affect DSB repair at this step, thereby causing the accumulation of γ-H2AX proteins. A recent study showed that CDKN1A proteins could inhibit the apoptosis of cancer cells by driving the expression of the pleiotrophin gene [24]. Based on this information, it was hypothesized that the miR-130b-mediated restriction of *CDKN1A* gene expression might drive cells into apoptosis, which was confirmed by the finding that the inhibition of the *CDKN1A* gene expression following transfection of either pSilencer: *CDKN1A* or miR-130b mimics into target cells increased the percentage of cells undergoing apoptosis, both at the early and late stages, whereas the increase in *CDKN1A* gene expression following the transfection of pcDNA3.1: *CDKN1A* vectors decreased the proportion of miR-130b-transfected cells undergoing apoptosis (Fig. **4D**). The cells undergo apoptosis *via* extrinsic and/or intrinsic pathways. In order to determine the mechanism underlying miR-130b-induced apoptosis in our study, the relative levels of caspase-8, -9, and -3 in the transfected cells were measured and compared. It showed that miR-130b could induce the cells at stationary phases *via* both the extrinsic and intrinsic pathways as the levels of both caspase 8 and 9 decreased in the cells transfected with miR-130bs as compared with NCs. Furthermore, the overexpression of CDKN1A proteins could increase the caspase 9 but not 8 levels significantly in miR-130b-transfected cells (Fig. **S5**). These data suggested that a CDKN1A protein could suppress miR-130b-induced apoptosis by blocking intrinsic cascades.

It has previously been shown that upregulated miR-130b-5p expression inhibits the growth of cervical cancer stem cells and promotes their apoptosis by decreasing the expression of the ETS transcription factor gene, ELK1. However, in the present study, it was shown that miR-130b-3p promoted the growth of cervical cancer cells and inhibited their apoptosis by reducing the expression of *CDKN1A* during the exponential phase. As presented in the

miRBase database, pri-miR-130b precursors are processed to generate a single dominant mature miRNA termed miR-130b-3p, along with a small proportion of reads originating from the opposite arm termed miR-130b-5p. The gene expression of miR-130b may serve dual roles in the development of cervical cancer and affect cell phenotypes based on the levels of miR-130b-5p and -3p since miR-130b-5p and -3p had different effects on the growth and survival of cervical cancer cells *via* regulation of different target genes. The role of a miRNA is not determined by a specific pathway or individual miRNA target but by large gene networks [25]. Therefore, the signaling pathways involving miR-130b may be significantly different between different cells used to study the function of miR-130b. As stem cells isolated from cervical cancer cells were employed in the previous study, whereas cervical cancer cells were used directly in the present study, it is hypothesized that miR-130b-5p exerts a more notable effect on the cell phenotype than miR-130b-3p in the stem cells of cervical cancer cells, whereas, in cervical cells, the effects of miR-130b-3p were more notable than miR-130b-5p.

## CONCLUSION

In the present study, it was shown that the gene expression levels of miR-130b were regulated by the methylation of a CpG island near the TSS of pri-miR-130b. An increase in miR-130b levels promoted the growth of cervical cancer cells during the exponential phase by negatively regulating the gene expression of CDKN1A, whereas a reduction in miR-130b levels sustained the survival of cells during the stationary phases.

## LIST OF ABBREVIATIONS

| | | |
|---|---|---|
| CDKN1A | = | Cyclin-dependent Kinase Inhibitor 1A |
| CIN | = | Cervical Intraepithelial Neoplasia |
| GEO | = | Gene Expression Omnibus |
| TSS | = | Transcript Start Site |
| Pri-miR-130b | = | Primary Transcript of miR-130b |
| $OD_{260nm}$ | = | Optical Density at 260 nm |
| DMSO | = | Dimethyl Sulfoxide |
| GFP | = | Green Fluorescent Protein |
| OTM | = | Oliver DNA Tail Moment |
| CASP | = | Comet Assay Software Project |
| DSB | = | Double Strand Break |

## ETHICS APPROVAL AND CONSENT TO PARTICIPATE

Not applicable.

## HUMAN AND ANIMAL RIGHTS

No animals/humans were used for studies that are the basis of this research.

## CONSENT FOR PUBLICATION

Not applicable.

## AVAILABILITY OF DATA AND MATERIALS

The nucleotide sequences of miR-130b and CDKN1A mRNA were respectively obtained from the miRBase database: a searchable database of published miRNA sequences and annotation at http://www.mirbase.org/ index.shtml and NCBI website at https://www.ncbi.nlm.nih.gov/gene/ [26]. The data describing the gene expression levels of miR-130b in cancer and normal cervical tissues in this article are available in the NCBI Gene Expression Omnibus (GEO): a public repository for a wide range of high-throughput microarray and next- generation sequence functional genomic datasets at https://www.ncbi.nlm.nih.gov/geo/query/acc.cgi?acc and data analysis were performed using the GEO2R online tool at https://www.ncbi.nlm.nih.gov/geo/geo2r/?acc [12]. The miR-130b-targeted genes were predicated online using three distinct bioinformatics algorithms at http://www.targetscan.org/vert_72/, http://www.microrna.org/microrna/home.do and http://diana.imis. athenainnovation.gr/DianaTools/index.ph p?r=tarbase/index. The TSS of pri-miR-130b was found using the FANTOM5 web tool and shown on a UCSC (hg38) genome viewer at https://genome.ucsc.edu/cgi-bin/hgTracks?db=hg38&lastVirtModeType=default&lastVirtModeExtraState=&virtModeType=default&virtMode=0&nonVirtPosition=&position=chr22%3A21565713%2D21569713&hgsid=1120218429_QZUMREbGdSxow5PziSeV6J0NtJad [27]. The CpG island was identified close to the TSS using the MethPrimer software at http://www.urogene.org/cgi-bin/methprimer2/MethPrimer.cgi.

## FUNDING

This work was supported by the National Natural Science Foundation of China (Nos. 81602403; 81470982).

## CONFLICT OF INTEREST

The author(s) declare no conflict of interests, financial or otherwise.

## ACKNOWLEDGEMENTS

Declared none.

## SUPPLEMENTARY MATERIAL

Supplementary material is available on the publisher's website along with the published article.

## REFERENCES

[1] Ferlay, J.; Colombet, M.; Soerjomataram, I.; Mathers, C.; Parkin, D.M.; Piñeros, M.; Znaor, A.; Bray, F. Estimating the global cancer incidence and mortality in 2018: GLOBOCAN sources and methods. *Int. J. Cancer,* **2019**, *144*(8), 1941-1953. http://dx.doi.org/10.1002/ijc.31937 PMID: 30350310

[2] Hoque, M.R.; Haque, E.; Karim, M.R. Cervical cancer in low-income countries: A Bangladeshi perspective. *Int. J. Gynaecol. Obstet.,* **2021**, *152*(1), 19-25.

http://dx.doi.org/10.1002/ijgo.13400 PMID: 32989750
[3] Vu, M.; Yu, J.; Awolude, O.A.; Chuang, L. Cervical cancer worldwide. *Curr. Probl. Cancer,* **2018**, *42*(5), 457-465. http://dx.doi.org/10.1016/j.currproblcancer.2018.06.003 PMID: 30064936
[4] Khan, S.; Ayub, H.; Khan, T.; Wahid, F. MicroRNA biogenesis, gene silencing mechanisms and role in breast, ovarian and prostate cancer. *Biochimie,* **2019**, *167*, 12-24. http://dx.doi.org/10.1016/j.biochi.2019.09.001 PMID: 31493469
[5] Gebert, L.F.R.; MacRae, I.J. Regulation of microRNA function in animals. *Nat. Rev. Mol. Cell Biol.,* **2019**, *20*(1), 21-37. http://dx.doi.org/10.1038/s41580-018-0045-7 PMID: 30108335
[6] Guo, Q.; Yan, J.; Song, T.; Zhong, C.; Kuang, J.; Mo, Y.; Tan, J.; Li, D.; Sui, Z.; Cai, K.; Zhang, J. microRNA-130b-3p contained in MSC-Derived EVs promotes lung cancer progression by regulating the FOXO3/NFE2L2/TXNRD1 axis. *Mol. Ther. Oncolytics,* **2020**, *20*, 132-146. http://dx.doi.org/10.1016/j.omto.2020.09.005 PMID: 33575477
[7] Mu, H.Q.; He, Y.H.; Wang, S.B.; Yang, S.; Wang, Y.J.; Nan, C.J.; Bao, Y.F.; Xie, Q.P.; Chen, Y.H. MiR-130b/TNF-α/NF-κB/VEGFA loop inhibits prostate cancer angiogenesis. *Clin. Transl. Oncol.,* **2020**, *22*(1), 111-121. http://dx.doi.org/10.1007/s12094-019-02217-5 PMID: 31667686
[8] Liao, Y.; Wang, C.; Yang, Z.; Liu, W.; Yuan, Y.; Li, K.; Zhang, Y.; Wang, Y.; Shi, Y.; Qiu, Y.; Zuo, D.; He, W.; Qiu, J.; Guan, X.; Yuan, Y.; Li, B. Dysregulated Sp1/miR-130b-3p/HOXA5 axis contributes to tumor angiogenesis and progression of hepatocellular carcinoma. *Theranostics,* **2020**, *10*(12), 5209-5224. http://dx.doi.org/10.7150/thno.43640 PMID: 32373208
[9] Huang, S.; Xue, P.; Han, X.; Zhang, C.; Yang, L.; Liu, L.; Wang, X.; Li, H.; Fu, J.; Zhou, Y. Exosomal miR-130b-3p targets SIK1 to inhibit medulloblastoma tumorigenesis. *Cell Death Dis.,* **2020**, *11*(6), 408. http://dx.doi.org/10.1038/s41419-020-2621-y PMID: 32483145
[10] Huang, Y.; Luo, F. Elevated microRNA-130b-5p or silenced ELK1 inhibits self-renewal ability, proliferation, migration, and invasion abilities, and promotes apoptosis of cervical cancer stem cells. *IUBMB Life,* **2021**, *73*(1), 118-129. http://dx.doi.org/10.1002/iub.2409 PMID: 33295145
[11] Yang, L.; Wang, Y.; Shi, S.; Xie, L.; Liu, T.; Wang, Y.; Mu, H. The TNF-α-induced expression of miR-130b protects cervical cancer cells from the cytotoxicity of TNF-α. *FEBS Open Bio,* **2018**, *8*(4), 614-627. http://dx.doi.org/10.1002/2211-5463.12395 PMID: 29632814
[12] Clough, E.; Barrett, T. The gene expression omnibus database. *Methods Mol. Biol.,* **2016**, *1418*, 93-110. http://dx.doi.org/10.1007/978-1-4939-3578-9_5 PMID: 27008011
[13] Livak, K.J.; Schmittgen, T.D. Analysis of relative gene expression data using real-time quantitative PCR and the 2(-Delta Delta C(T)) Method. *Methods,* **2001**, *25*(4), 402-408. http://dx.doi.org/10.1006/meth.2001.1262 PMID: 11846609
[14] Yang, C.; Cai, J.; Wang, Q.; Tang, H.; Cao, J.; Wu, L.; Wang, Z. Epigenetic silencing of miR-130b in ovarian cancer promotes the development of multidrug resistance by targeting colony-stimulating factor 1. *Gynecol. Oncol.,* **2012**, *124*(2), 325-334. http://dx.doi.org/10.1016/j.ygyno.2011.10.013 PMID: 22005523
[15] Olive, P.L.; Banáth, J.P. The comet assay: A method to measure DNA damage in individual cells. *Nat. Protoc.,* **2006**, *1*(1), 23-29. http://dx.doi.org/10.1038/nprot.2006.5 PMID: 17406208
[16] Końca, K.; Lankoff, A.; Banasik, A.; Lisowska, H.; Kuszewski, T.; Góźdź, S.; Koza, Z.; Wojcik, A. A cross-platform public domain PC image-analysis program for the comet assay. *Mutat. Res.,* **2003**, *534*(1-2), 15-20. http://dx.doi.org/10.1016/S1383-5718(02)00251-6 PMID: 12504751
[17] Sharma, A.; Singh, K.; Almasan, A. Histone H2AX phosphorylation: A marker for DNA damage. *Methods Mol. Biol.,* **2012**, *920*, 613-626. http://dx.doi.org/10.1007/978-1-61779-998-3_40 PMID: 22941631
[18] De Biasio, A.; Blanco, F.J. Proliferating cell nuclear antigen structure and interactions: Too many partners for one dancer? *Adv. Protein Chem. Struct. Biol.,* **2013**, *91*, 1-36. http://dx.doi.org/10.1016/B978-0-12-411637-5.00001-9 PMID: 23790209
[19] Wiese, C.; Rudolph, J.H.; Jakob, B.; Fink, D.; Tobias, F.; Blattner, C.; Taucher-Scholz, G. PCNA-dependent accumulation of CDKN1A into nuclear foci after ionizing irradiation. *DNA Repair (Amst.),* **2012**, *11*(5), 511-521. http://dx.doi.org/10.1016/j.dnarep.2012.02.006 PMID: 22456500
[20] El-Deiry, W.S. p21(WAF1) mediates cell-cycle inhibition, relevant to cancer suppression and therapy. *Cancer Res.,* **2016**, *76*(18), 5189-5191. http://dx.doi.org/10.1158/0008-5472.CAN-16-2055 PMID: 27635040
[21] Dutto, I.; Tillhon, M.; Prosperi, E. Assessing cell cycle independent function of the CDK inhibitor p21(CDKN¹A) in Dna repair. *Methods Mol. Biol.,* **2016**, *1336*, 123-139. http://dx.doi.org/10.1007/978-1-4939-2926-9_11 PMID: 26231713
[22] Yang, L.; Yang, B.; Wang, Y.; Liu, T.; He, Z.; Zhao, H.; Xie, L.; Mu, H. The CTIP-mediated repair of TNF-α-induced DNA double-strand break was impaired by miR-130b in cervical cancer cell. *Cell Biochem. Funct.,* **2019**, *37*(7), 534-544. http://dx.doi.org/10.1002/cbf.3430 PMID: 31418900
[23] Jakob, B.; Scholz, M.; Taucher-Scholz, G. Characterization of CDKN1A (p21) binding to sites of heavy-ion-induced damage: Colocalization with proteins involved in DNA repair. *Int. J. Radiat. Biol.,* **2002**, *78*(2), 75-88. http://dx.doi.org/10.1080/09553000110090007 PMID: 11779358
[24] Huang, P.; Ouyang, D.J.; Chang, S.; Li, M.Y.; Li, L.; Li, Q.Y.; Zeng, R.; Zou, Q.Y.; Su, J.; Zhao, P.; Pei, L.; Yi, W.J. Chemotherapy-driven increases in the CDKN1A/PTN/PTPRZ1 axis promote chemoresistance by activating the NF-κB pathway in breast cancer cells. *Cell Commun. Signal.,* **2018**, *16*(1), 92. http://dx.doi.org/10.1186/s12964-018-0304-4 PMID: 30497491
[25] Han, Y.C.; Vidigal, J.A.; Mu, P.; Yao, E.; Singh, I.; González, A.J.; Concepcion, C.P.; Bonetti, C.; Ogrodowski, P.; Carver, B.; Selleri, L.; Betel, D.; Leslie, C.; Ventura, A. An allelic series of miR-17 ~ 92-mutant mice uncovers functional specialization and cooperation among members of a microRNA polycistron. *Nat. Genet.,* **2015**, *47*(7), 766-775. http://dx.doi.org/10.1038/ng.3321 PMID: 26029871
[26] Kozomara, A.; Birgaoanu, M.; Griffiths-Jones, S. miRBase: From microRNA sequences to function. *Nucleic Acids Res.,* **2019**, *47*(D1), D155-D162. http://dx.doi.org/10.1093/nar/gky1141 PMID: 30423142
[27] Haeussler, M.; Zweig, A.S.; Tyner, C.; Speir, M.L.; Rosenbloom, K.R.; Raney, B.J.; Lee, C.M.; Lee, B.T.; Hinrichs, A.S.; Gonzalez, J.N.; Gibson, D.; Diekhans, M.; Clawson, H.; Casper, J.; Barber, G.P.; Haussler, D.; Kuhn, R.M.; Kent, W.J. The UCSC Genome Browser database: 2019 update. *Nucleic Acids Res.,* **2019**, *47*(D1), D853-D858. http://dx.doi.org/10.1093/nar/gky1095 PMID: 30407534